ResearchGate

See discussions, stats, and author profiles for this publication at: https://www.researchgate.net/publication/279633924

Exhibit
G26

Coalescing Wind Turbine Wakes

Article *in* Journal of Physics Conference Series · June 2015

DOI: 10.1088/1742-6596/625/1/012023

CITATION
1

READS
105

7 authors, including:

Sang Lee
University of New Mexico
41 PUBLICATIONS **1,004** CITATIONS
SEE PROFILE

Senu Sirnivas
National Renewable Energy Laboratory
13 PUBLICATIONS **64** CITATIONS
SEE PROFILE

Patrick J. Moriarty
National Renewable Energy Laboratory
90 PUBLICATIONS **1,819** CITATIONS
SEE PROFILE

Finn Gunnar Nielsen
University of Bergen
53 PUBLICATIONS **612** CITATIONS
SEE PROFILE

All content following this page was uploaded by Patrick J. Moriarty on 08 July 2015.

The user has requested enhancement of the downloaded file.

IOPscience iopscience.iop.org

Home Search Collections Journals About Contact us My IOPscience

Coalescing Wind Turbine Wakes

This content has been downloaded from IOPscience. Please scroll down to see the full text.

2015 J. Phys.: Conf. Ser. 625 012023

(http://iopscience.iop.org/1742-6596/625/1/012023)

View the table of contents for this issue, or go to the journal homepage for more

Download details:

IP Address: 192.174.37.50
This content was downloaded on 08/07/2015 at 21:13

Please note that terms and conditions apply.

Coalescing Wind Turbine Wakes

S Lee[1a], M. Churchfield[a], S. Sirnivas[a], P. Moriarty[a], F. G. Nielsen[b,c], B. Skaare[b], and E. Byklum[b]
[a]National Renewable Energy Laboratory, Golden, CO, U.S.A.
[b]Statoil, Norway
[c]University of Bergen, Geophysical Institute

E-mail: Sang.Lee@nrel.gov

Abstract. A team of researchers from the National Renewable Energy Laboratory and Statoil used large-eddy simulations to numerically investigate the merging wakes from upstream offshore wind turbines. Merging wakes are typical phenomena in wind farm flows in which neighboring turbine wakes consolidate to form complex flow patterns that are as yet not well understood. In the present study, three 6-MW turbines in a row were subjected to a neutrally stable atmospheric boundary layer flow. As a result, the wake from the farthest upstream turbine conjoined the downstream wake, which significantly altered the subsequent velocity deficit structures, turbulence intensity, and the global meandering behavior. The complexity increased even more when the combined wakes from the two upstream turbines mixed with the wake generated by the last turbine, thereby forming a "triplet" structure. Although the influence of the wake generated by the first turbine decayed with downstream distance, the mutated wakes from the second turbine continued to influence the downstream wake. Two mirror-image angles of wind directions that yielded partial wakes impinging on the downstream turbines yielded asymmetric wake profiles that could be attributed to the changing flow directions in the rotor plane induced by the Coriolis force. The turbine wakes persisted for extended distances in the present study, which is a result of low aerodynamic surface roughness typically found in offshore conditions.

1. Introduction

Turbine wakes interacting with neighboring wakes is a complex physical process that significantly impacts not only the global energy capture of an operational wind farm but the longevity of the individual turbines, which leads to uncertainty in the cost of energy during a 20-year design life. Although empirically formulated turbulence intensity models exist to predict the fatigue life of turbines placed within an array, inaccuracies are thought to have led to stringent designs that ultimately sacrifice the turbines' overall economic competiveness. Even more perplexing is the lack of understanding of the influence on the power and loads of merging turbine wakes within wind farms. Therefore, in the present study, we aimed to characterize the mean wake deficits, turbulent kinetic energy produced by merged wakes, and their altered configurations caused by varying wind directions.

2. Numerical Methodology

During this study, a team of researchers from the National Renewable Energy Laboratory (NREL) and Statoil performed large-eddy simulations (LES) of the atmospheric boundary layer with three 6-MW, three-bladed, horizontal-axis wind turbines placed in a row. To accomplish this, we used an

[1] To whom any correspondence should be addressed.

Content from this work may be used under the terms of the Creative Commons Attribution 3.0 licence. Any further distribution of this work must maintain attribution to the author(s) and the title of the work, journal citation and DOI.
Published under licence by IOP Publishing Ltd

incompressible formulation of the continuity equation (Eq. 1) and the momentum equation (Eq. 2), which includes the Coriolis force, buoyancy force, and aerodynamic force at the actuator point, and the potential temperature transport equations (Eq. 3). These equations are shown in the following:

$$\frac{\partial u_i}{\partial x_i} = 0 \tag{1}$$

$$\frac{\partial u_i}{\partial t} + \frac{\partial}{\partial x_j}(u_i u_j) = -\frac{\partial \hat{p}}{\partial x_i} - \frac{\partial \tau_{ij}^D}{\partial x_j} - \frac{1}{\rho_0}\frac{\partial p_0(x,y)}{\partial x_i} - \varepsilon_{i3k} f_3 u_k + g\left(\frac{\theta-\theta_0}{\theta_0}\right)\delta_{i3} + \frac{1}{\rho_0}F_i \tag{2}$$

$$\frac{\partial \theta}{\partial t} + \frac{\partial}{\partial x_j}(u_j\theta) = \frac{\upsilon_{SGS}}{Pr_{SGS}}\frac{\partial^2\theta}{\partial x_j^2} \tag{3}$$

Note that all of the primitive variables are spatially resolved components. The modified pressure is defined as $\hat{p} = p'/\rho_0 + \frac{\tau_{kk}}{3}$, where $p'(x,y,z,t) = p(x,y,z,t) - p_0(x,y) + \rho_0 gz$. The filtered static pressure term is p, and ρ_o is the constant density. The mean pressure term is $p_0(x,y)$, in which the spatial gradient acts to drive the flow convection. The last term, $\rho_0 gz$, represents the hydrostatic pressure. The deviatoric part of the fluid stress tensor is $\tau_{ij}^D = \tau_{ij} - \tau_{kk}\delta_{ij}/3$, where δ_{ij} is the Kronecker delta. The subgrid-scale (SGS) stresses are included in the τ_{ij} term. The SGS flux is computed using the dynamic Lagrangian scale-independent model [1]. The ε_{ijk} is the alternating unit tensor. The Coriolis parameter is defined as $f = 2\omega[0, \cos(\varphi), \sin(\varphi)]$, where ω is the planetary rotation rate ($7.27\text{x}10^{-5}$ rad/s) and φ (43.2^o) is the latitude. Coriolis forces are important because they cause a mean wind direction change with height described by Ekman spiral/transport theory. Including this effect is essential because the mean wind direction change over the rotor disk can be a significant contributor to cyclic blade loading that causes fatigue, especially during stable atmospheric conditions. The buoyancy effect is calculated using the Boussinesq approximation, where g is the gravity, θ is the resolved potential temperature, θ_0 is the reference temperature taken to be 300 K. The last term, F_i, is the force field generated by the actuator line model, which is discussed in the following section. The transport equation for the potential temperature is shown in (3) where υ_{SGS} and Pr_{SGS} are the SGS viscosity and turbulent Prandtl number following Moeng's formulation [2].

The turbine model consists of an actuator line representation of the turbine blades coupled with NREL's computer-aided engineering tool FAST [3]. FAST employs a combined modal and multibody dynamics formulation. Within FAST, each turbine blade is represented by a set of discrete elements along the blade that move in space as the turbine blades rotate and bend. The tool then uses the local flow field at each blade element to compute aerodynamic forces, via the dynamic airfoil coefficient lookup tables in the AeroDyn module [4]. Using the updated blade-element positions, the aerodynamic forces are projected onto the flow field as a body force term in the LES equation. Therefore, this actuator line representation consists of two-way coupling, in which the flow information is used as an input to compute the aerodynamic forces that are pressed on to the flow with new positions.

The preceding equations addressing the incompressible Navier-Stokes with the Coriolis force and the potential temperature flux are solved using Simulator fOr Wind Farm Applications, which is the NREL LES code [5] that was developed using OpenFOAM libraries. The equations are discretized using an unstructured collocated finite-volume formulation. The second-order central-differencing scheme is employed and uses the Rhie and Chow interpolation method [6] to avoid checkerboard pressure-velocity decoupling. For the time advancement, pressure implicit with splitting operation [7] is used, with three substep corrections to maintain a second-order temporal accuracy. FAST's aeroelastic calculation employs the fourth-order Adams-Bashforth predictor and Adams-Moulton corrector time integration scheme.

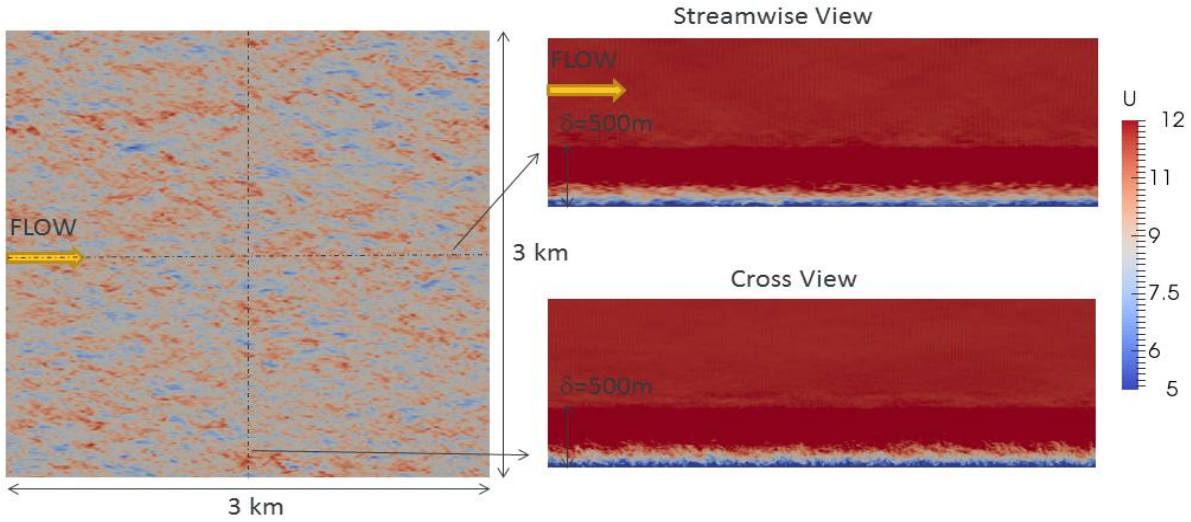

Figure 1. Instantaneous streamwise velocity contours from the precursor simulation.

The turbulent inflow boundary condition is generated via a precursor simulation. In this study, the size of the precursor computational domain was set at 3 km x 3 km x 1 km to accommodate a wide range of length scales of the turbulent structures. The grid resolution was fixed with a 10-m uniform mesh and the driver for the wind was based on the pressure gradient to obtain a mean wind speed of 10.4 m/s at the turbine hub height (z = 98.2-m). The turbulence intensity was adjusted to 4.2% of the freestream flow with an aerodynamic surface roughness of 0.0002 m. The same pressure gradient was used for the turbine simulations because the changes in the surface roughness were moderately small. The atmospheric stability was neutral by fixing the potential temperature flux at the surface to be zero. Samples of the instantaneous streamwise velocity contours at various locations are provided in Figure 1, which shows the boundary layer height, δ, at approximately 500 m.

3. Computational Domain

The LES study was performed using a domain extended in the general wind direction to accommodate

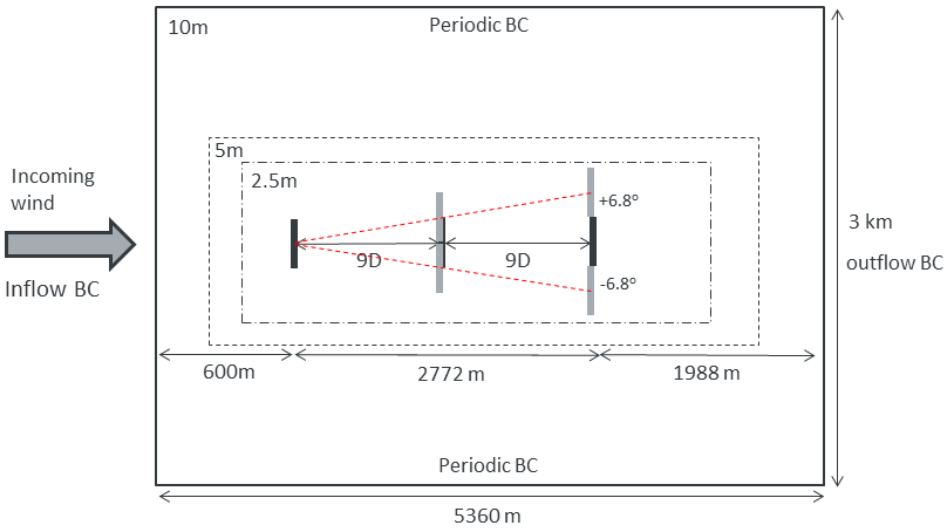

Figure 2. Computational domain schematic.

three turbines that are separated by 9 rotor diameters (D). As shown in Figure 2, two layers of grid nesting were created within the existing 10-m resolution grid to better capture the turbine wake structures that yielded a 2.5-m resolution in the subdomain where the turbines are embedded. The total number of cells was approximately 80 million. The turbulent inflow boundary condition was imposed at the west boundary with the precursor database. An outflow boundary condition on the east boundary allowed the turbulent structures to smoothly exit the domain and enforce zero-net-mass conservation per numerical time step. The north and south boundaries are connected via periodic boundary conditions, which yielded a minimal effect on the turbine wake propagation as a result of the far distance. The generic, 6-MW offshore turbine has a rotor diameter of 154 m and its structural and aerodynamic properties were modeled in FAST. Change in wind direction is mimicked by rotating the turbine row by $\pm 6.8^{o}$ relative to the first turbine.

4. Results

4.1. Wind direction at 270^{o}

Figure 3 shows three wind turbines in a row subjected to a neutrally stable atmospheric boundary layer flow, in which both the instantaneous velocity contours of the streamwise and vertical components (Figure 3a and 3c, respectively) exhibit significant wake meandering motions where the wake structure randomly traverses in lateral directions [8, 9]. As shown in the instantaneous velocity contours, the meandering of the wake becomes worse at each passing of downstream turbines, which is attributed to increased turbulent mixing incurred by the interaction between the waked inflow and rotors. Increased wake diffusion is clearly observed in the transverse velocity contour (Figure 3c), where the wake width spreads significantly along the downstream distance. In the time-averaged streamwise velocity contour shown in Figure 3b, the wake deficit regions still persist, even at a 9-D

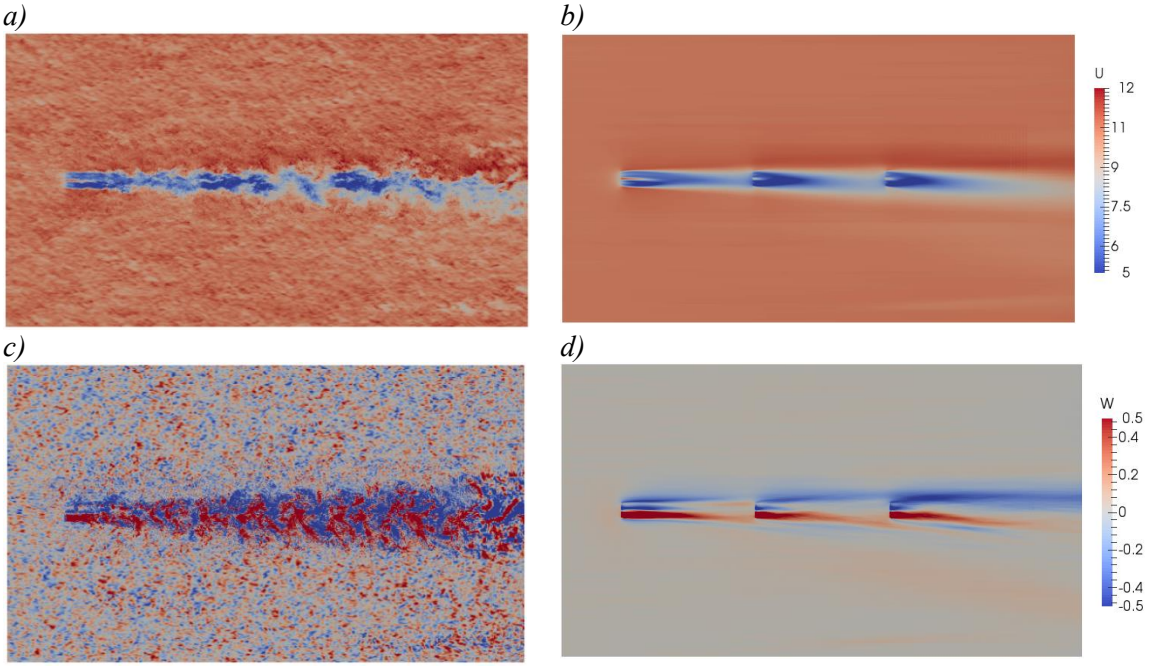

Figure 3. Instantaneous (left column) and time-averaged (right column) velocity contours of streamwise (U: a – b) and vertical (W: c – d) components. The mean freestream velocity at hub height is 10.4 m/s.

distance, where the adjacent turbines are located; however, the recovery of the velocity deficit is improved for turbine 2 and 3, even though the velocity deficits are stronger in the near wake regions. The wake structure, in general, rotates counter-clockwise in the opposite direction to the blade rotation. As shown in Figure 3c and 3d, consistent updrafts are present on the right region when looking downstream and, conversely, down drafts are prevalent on the left region.

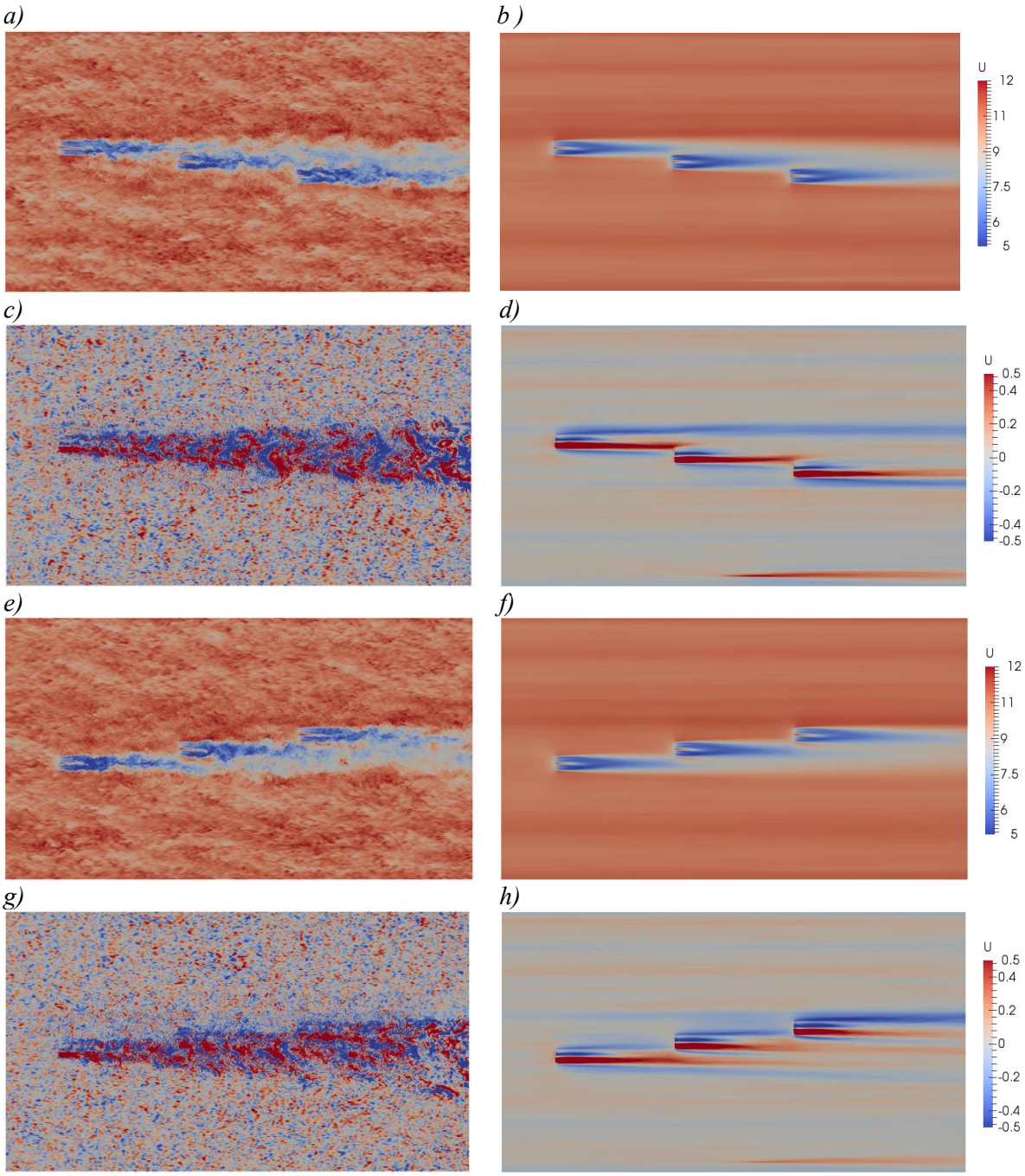

Figure 4. Instantaneous (left column) and time-averaged (right column) velocity contours of streamwise (U) and vertical (W) components for the 263.2^{o} wind direction: a) – d) and 276.8^{o} wind direction: e) – h).

4.2. Wind directions at 263.2^o and 276.8^o

A 6.8^o shift in the wind direction from the previous case is mimicked by rotating the turbine row by ±6.8^o relative to the freestream wind at 270^o, which are shown in Figure 4. The skewed wind direction resulted in a partial waking for the downstream turbines, in which approximately half of the upstream turbine wake impinged on the downstream rotor plane. Parcels of low-speed fluid that avoided contact with the downstream rotor plane can be seen to convect past the downstream turbines as shown in Figure 4a and 4e. Note that the meandering wake is mitigated for the second turbine compared to the fully waked case shown in Figure 3a, which is attributed to less turbulent mixing.

Figure 5 shows cross-cut planes of time-averaged streamwise velocity contours looking upstream of the flow for the 263.2^o case and the 276.8^o case. The relative positions, with respect to the immediate upstream turbine locations, were taken at 3, 5 and 7 rotor diameters downstream. The primary wake structures exhibit ellipsoidal shapes in which the blue regions shown at 3 D are seen to reduce in size at 7 D. A small footprint of the wake from the upstream turbine can be found in the right region of the primary wake for the 263.2^o case as shown in Figure 5a through Figure 5f. Conversely, the secondary

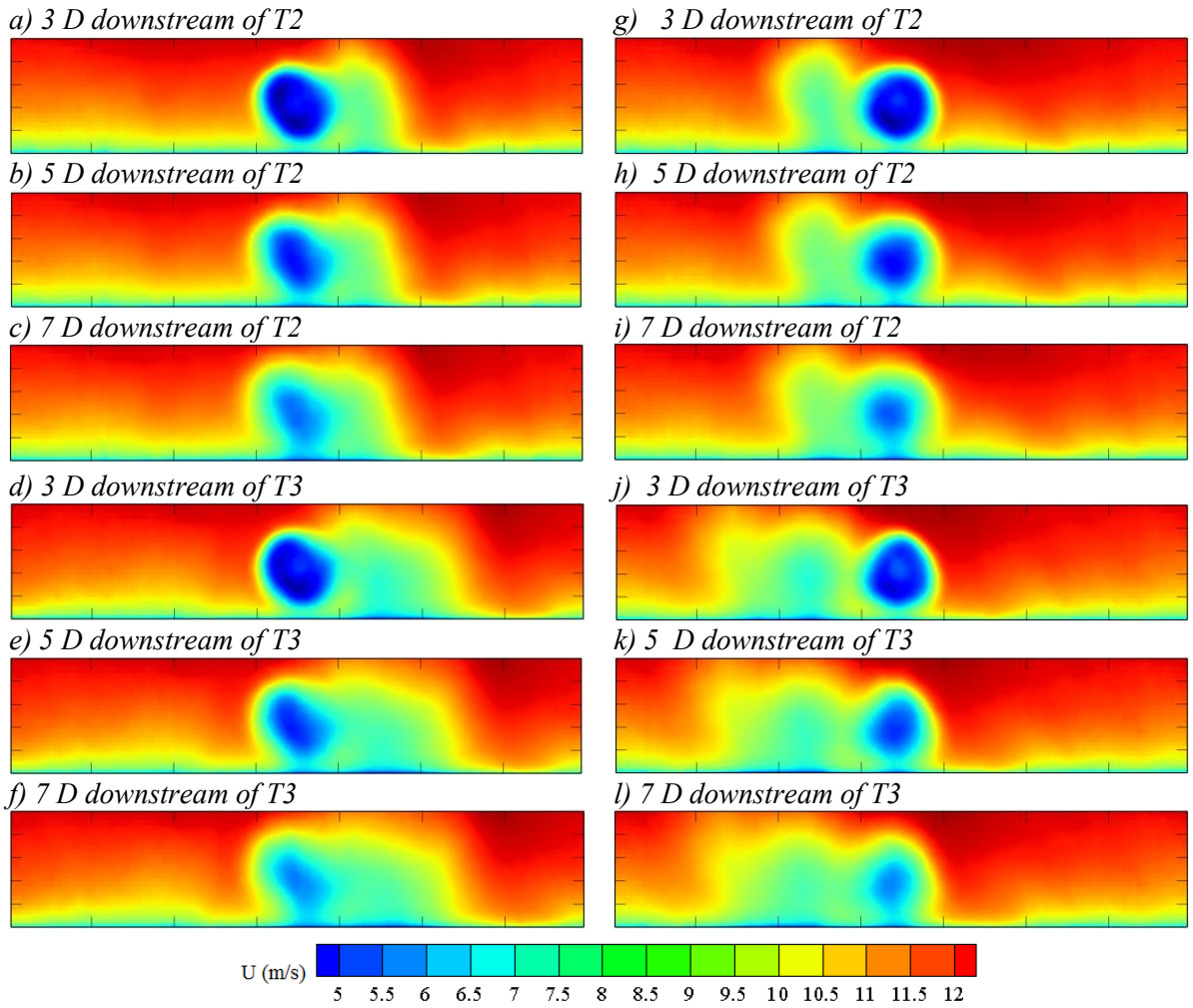

Figure 5. Cross-cut view of time-averaged streamwise velocity contours for 263.2^o (left column) and 276.8^o (right column). The relative positions, with respect to the immediate upstream turbine locations, are described in the figure subindex.

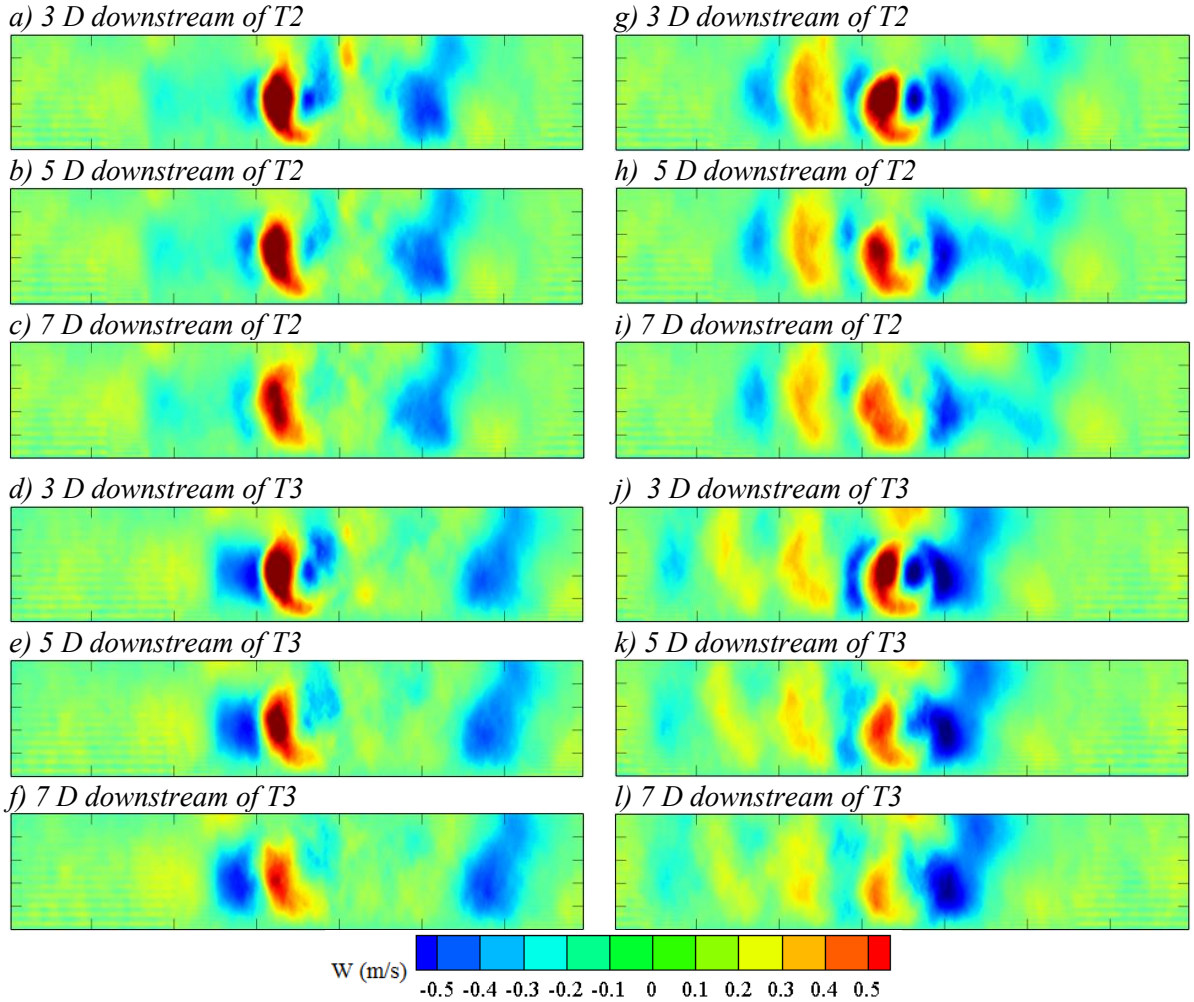

Figure 6. Cross-cut view of time-averaged vertical velocity contours for 263.2° (left column) and 276.8° (right column). The relative positions, with respect to the immediate upstream turbine locations, are described in the figure subindex.

wake structures present on the left side of the primary wake in Figure 5g through Figure 5l can be seen for the 276.8° case and they are more circular than the opposite wind direction. We speculate that the asymmetry in the wake deficit regions is a result of the Coriolis effect, which skews the wake structure by flow directional change that is combined with the merging wakes that rotate. The persistence of the multiple wake structure can be detrimental to the downwind turbines' energy production and fatigue damage.

The time-averaged, vertical velocity contours at the same locations are shown in Figure 6. The updraft and downdraft regions denoted in red and blue are clearly shown, suggesting that the wake structure continues to slowly rotate further downstream. Despite the viscous effect that causes the wake to dissipate along the downstream distance, the rotating wake structure from the previous upstream turbines persist which are shown as light blue and yellow structure pairs. The extended survivability of the upstream wake structures can be attributed to the relatively low ambient turbulence intensity. Note that in the 276.8° case, the upstream wake structures appear more visible than in the 263.2° case.

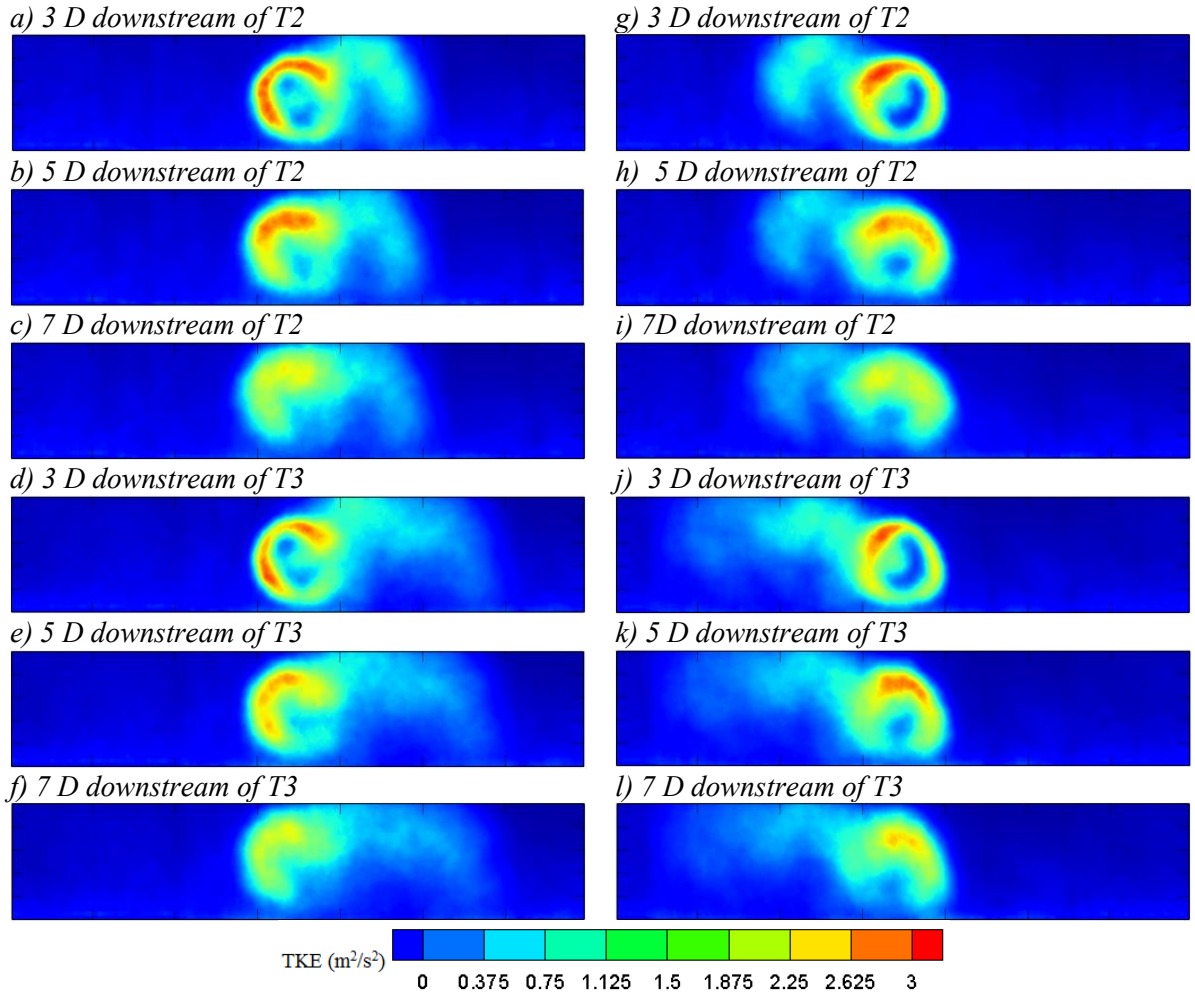

Figure 7. Cross-cut view of time-averaged turbulent kinetic energy contours for 263.2° (left column) and 276.8° (right column). The relative positions, with respect to the immediate upstream turbine locations, are described in the figure subindex.

The turbulent kinetic energy contours reveal that high intensity regions are mostly found at the circumferential edge of the primary wake structure because of the high shear in the flow. The lack of a nacelle model in the actuator line method attributed to the low turbulent kinetic energy at the centroid of the primary wake region. As expected, the merging wakes from the far upstream turbine have lower turbulent kinetic energy. It is worth noting that the wake signatures from the two upstream turbines are still present, yet they have diffused and decayed in intensity.

5. Conclusions

Large-eddy simulations of three 6-MW, three-bladed, horizontal-axis turbines subjected to a neutral atmospheric boundary layer flow were performed with three different wind directions. By imparting the turbine arrays to 263.2°, 270°, and 276.8° wind direction, the resulting flow yielded different wake longevity and merging scenarios. One extreme case was the 270° wind direction simulation, in which the persisting wake was fully merged with the wakes generated by the downstream turbines. The meandering of the wake's tail significantly increased with each passing rotor plane as a result of higher levels of turbulent mixing from each subsequent turbine. By shifting the wind direction by

±6.8°, we found that the footprints of the wake continued to propagate further past the turbines that were spaced at 9 D; however, the persisting lengths of the wake structure were shown to have asymmetric results in which the 263.2° case exhibited wakes from the previous upstream turbine to partially mix with the adjacent primary wake structure, causing the wake rotation to decay quickly. Conversely, the 276.8° case was able to capture triplet wake structures at 7 D downstream from the third turbine. Despite the symmetry in the two wind directions, the varying flow direction with respect to the height in the boundary layer caused by the Coriolis force appeared to dominantly influence the asymmetry in the wake development. Various conditions including atmospheric stability, aerodynamic surface roughness, and mean wind speed, which drive the turbulent mixing in the boundary layer, dominantly influence the level of asymmetric wake propagation and should be better quantified in future research. This asymmetric behavior of wake propagation can have significant implications with respect to the energy capture and fatigue damage that accumulates over a wind turbine's service lifetime, which should be accounted for when designing wind farms.

6. Acknowledgments

The authors gratefully acknowledge the funding support provided by Statoil and the Department of Energy. All the computations were performed on the Peregrine of the National Renewable Energy Laboratory and on the Hexagon of the University of Bergen's high-performance computing system. The authors also thank the project team members for their insightful discussions: Jim Green, Zachary Parker, Aaron Smith, Andrew Platt, George Scott, Tyler Stehly, Donna Heimiller, Pieter Gebraad and Paul Fleming from the National Renewable Energy Laboratory and Andrea Nina Eugster from Statoil and Michelle Burns and Nick Wimer from the University of Colorado at Boulder.

7. References

[1] Meneveau C, Lund T and Cabot W 1996 *A lagrangian dynamic subgrid-scale model of turbulence*, J. Fluid Mech. **319**, pp. 353-385
[2] Moeng C H 1984 *A large eddy simulation model for the study of planetary boundary layer turbulence*, J. Atmospheric Sciences, **41**, pp. 2052-2062
[3] Jonkman J M and Buhl M L 2005 *FAST User's Guide*, NREL/EL-500-3823
[4] Moriarty P J and Hansen A C 2005 *AeroDyn Theory Manual*, NREL/EL-500-36881
[5] *Simulator fOr Wind Farm Applications*, http://wind.nrel.gov/designcodes/simulators/sowfa/
[6] Rhie C M and Chow W L 1983 *Numerical Study of the Turbulent Flow Past an Airfoil with Trailing Edge Separation*, AIAA J. **21**, pp. 1525-1532
[7] Issa R 1985 *Solution of the implicitly discretized fluid flow equations by operator-splitting*, J. Comput. Phys., **62**, pp. 40–65
[8] Larsen G C, Madsen H A, Bing¨ol F, Mann J, Ott S, Sørensen J N, Okulov V, Troldborg N, Nielsen M, Thomsen K, Larsen T J and Mikkelsen R 2007 *Dynamic Wake Meandering Modeling*, Tech. Rep. R-1607(EN), Risø National Laboratory, Technical University of Denmark, Roskilde, Denmark
[9] Larsen G C, Madsen H A, Thomsen K and Larsen T J 2008 *Wake Meandering – A Pragmatic Approach*, Wind Energy, Vol. 11, No. 4, pp. 377–395

View publication stats